Matter-Wave Self-Imaging by Atomic Center-of-Mass Motion Induced Interference

Ke Li,[1,2,3] L. Deng,[1] E. W. Hagley,[1] M. G. Payne,[1] and M. S. Zhan[2,3]

[1]*Physics Laboratory, National Institute of Standards and Technology, Gaithersburg, Maryland 20899, USA*

[2]*State Key Laboratory of Magnetic Resonance, Atomic and Molecular Physics, Wuhan Institute of Physics and Mathematics, Chinese Academy of Sciences, Wuhan 430071, China*

[3]*Center for Cold Atom Physics, Chinese Academy of Sciences, Wuhan 430071, China*

(Received 25 August 2008; published 18 December 2008)

We demonstrate matter-wave self-imaging resulting from atomic center-of-mass motion-based interference. We show that non-negligible atomic center-of-mass motion and an instantaneous Doppler shift can drastically change the condensate momentum distribution, resulting in a periodic collapse and the recurrence of condensate diffraction probability as a function of the stationary light-field pulsing time. The observed matter-wave self-imaging is characterized by an atomic center-of-mass motion induced population amplitude interference in the presence of the light field that simultaneously minimizes all high ($n \geq 1$) diffraction orders and maximizes the zeroth diffraction component.

DOI: 10.1103/PhysRevLett.101.250401 PACS numbers: 03.75.−b, 42.25.Fx, 67.85.Hj

Deflection and diffraction of atoms by light is a research area that can be traced back more than 40 years to early pioneering theoretical and experimental studies [1–11]. The recent development of laser cooling and trapping technology, and the realization of Bose-Einstein condensates (BECs), have greatly advanced the research activities of coherent atom optics, a rapidly developing new research area of modern atomic physics. In comparison with thermal atomic sources, atomic BECs as atom-optical sources have the advantages of high phase space density and high spatial localization, and are therefore well suited for high resolution time-domain matter-wave diffraction studies. Indeed, various groups have demonstrated Bragg diffraction of condensates [12,13], pulsed standing-wave diffraction of a condensate [14], the time-domain matter-wave Talbot effect [15], condensate coherence-time measurements [16], Bragg-diffraction-based quasicontinuous atom lasers [17], and coherent matter-wave mixing [18].

Diffraction of ultracold atoms by optical standing waves usually can be classified into two time regimes. In the Raman-Nath regime the optical standing wave is pulsed for a very short time so that the atom center-of-mass (c.m.) motion and instantaneous Doppler frequency shift can be neglected [2,14–16]. The characteristic bidirectional momentum distribution of the diffracted ultracold atoms and BEC components is well described by Bessel functions evenly distributed on both sides of the zero momentum component. In the Bragg regime, the optical grating is pulsed for a much longer time, and the stringent phase matching condition results in a unidirectional diffraction pattern.

In this Letter using an optical standing wave formed with counterpropagating beams of significant intensity difference we demonstrate atomic c.m. motion-based bidirectional, high-order matter-wave self-imaging and condensate momentum oscillation. This phenomenon exists in the non-Raman-Nath regime that is also far away from the typical Bragg regime. We further note that the matter-wave self-imaging effect reported here is not related to the temporal, matter-wave Talbot effect reported previously [15]. To the best of our knowledge, such a full matter-wave self-imaging resulting from atomic c.m. motion induced interference has never been demonstrated before.

The experiment reported here was performed with a ^{87}Rb condensate in the $|F = 2, m_F = 2\rangle$ hyperfine ground state. We first collect 10^8 atoms in a double magneto-optical trap and transfer the cold atoms into a quadrupole-Ioffe-configuration trap for further evaporative cooling, producing an almost pure condensate that typically contains 10^5 atoms. We expand the condensate for 3 ms [19] and then illuminate the condensate with a pair of counterpropagating laser pulses of selected pulse duration and uneven intensities. In our setup the pulsed standing-wave light fields are applied along the long dimension of the condensate (Fig. 1). The strong pump field (wave vector $\hat{k}_1 = \hat{k}_L$, $I_1 \approx 215$ mW/cm^2) propagates in the $+\hat{x}$ direction, whereas a much weaker pump field (wave vector $\hat{k}_2 = -\hat{k}_L$, $I_2 \approx 14$ mW/cm^2) propagates collinearly in the $-\hat{x}$ direction. Both fields come from the same laser (wavelength $\lambda_L = 780$ nm) that is linearly polarized in $\hat{z}$ direction, detuned $\Delta = 2\pi(-1.5)$ GHz below the $F' = 3$, $m_{F'} = 2$ state [20], and locked to a saturation absorption cell maintained under constant temperature. Immediately after irradiation by the pump laser pulses we allow 30 ms of ballistic expansion of the condensate before imaging its momentum distribution with on-resonance light.

In Fig. 2 we show a series of images of condensate momentum distribution for different standing-wave pulse durations. In obtaining these images, we have used optical powers of 20 and 1.3 mW for the two pump fields (beam radius $r_{1/e} \approx 1.7$ mm), respectively. The images are taken after a 30 ms time of flight. With a 1 μs pump pulse the condensate momentum distribution has only the $p = 0\hbar k_L$

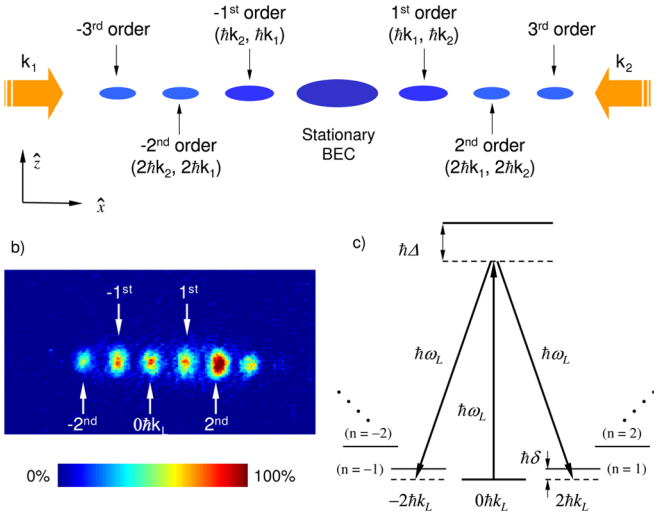

FIG. 1 (color online). (a) Schematics of experiment setup and directions of laser propagation. (b) A typical diffraction image obtained after about 30 ms time of flight. (c) Schematic energy-level diagram and laser couplings used in deriving Eq. (1).

component. After a 6 μs pulse more condensate components of nonzero momenta have developed and we observe the depletion of the $0\hbar k_L$ component. After an 8 μs pulse the zero momentum component is repopulated. At 25 μs, however, populations in all high-order momentum components are very small in comparison with the stationary condensate ($0\hbar k_L$). That is, the condensate momentum distribution has collapsed completely and matter-wave self-imaging is achieved. As the standing-wave pulse time is further increased, the multiorder bidirectional condensate momentum diffraction distribution reappear. At

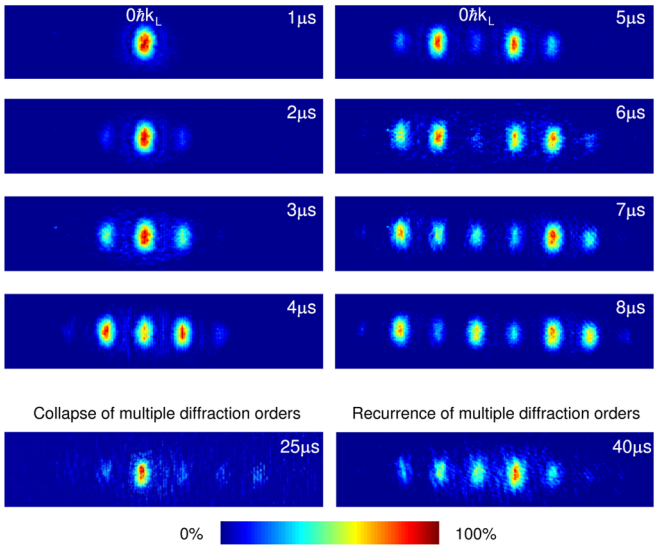

FIG. 2 (color online). Matter-wave self-imaging and condensate momentum distribution collapse and recurrence in a pulsed optical standing wave. Field of view: 2.7 mm × 0.63 mm (see text for other parameters) and condensate time of flight is typically 30 ms.

40 μs the bidirectional high-order momentum distributions are clearly seen.

To explain the observed condensate momentum distribution collapse, recurrence, and matter-wave self-imaging observed near $\tau_P \approx 25$ μs, we consider an atomic system that includes two electronic states and n momentum states [Fig. 1(c)] [20]. In the rest frame of an atom each two-photon process that involves absorption of one photon from one beam and emission of one photon to the other beam leads to the atom, which has mass M and was initially at rest, acquiring a velocity $V_r = \pm 2\hbar k_L/M$, which results in a two-photon recoil energy $E_r/\hbar = \delta = 2\hbar k_L^2/M = 8\pi\nu_r$, where $\nu_r = \hbar k_L^2/(4\pi M)$ is the one-photon recoil frequency. The atomic c.m. motion thus leads to an instantaneous Doppler shift in angular frequency $\Delta\omega_{\text{Doppler}} = 2(2n\hbar k_L)\omega_L/(Mc) = 4n\hbar k_L^2/M = 16\pi n\nu_r$ ($n = 0, \pm 1, \pm 2, \ldots$). The equation of motion of the probability amplitude of the nth momentum state of the atomic ground electronic state wave function for such a standing wave formed by counterpropagating beams of significant intensity difference can be written as [21] (see discussion on asymmetry later)

$$\Psi_n(p;t) = iZ[\Psi_{n-1}e^{-i\delta_- t} + \Psi_{n+1}e^{-i\delta_+ t}], \qquad (1)$$

where $\delta_\pm = \delta \pm \Delta\omega_{\text{Doppler}} = \pm 16\pi\nu_r(n \pm \frac{1}{2})$. The real quantity $Z = \Omega_1\Omega_2/\Delta$ is the two-photon Rabi frequency, $\Omega_j = \Gamma\sqrt{I_j/(2I_s)}$ (with $\Gamma = 2\pi \times 6.07$ MHz and $I_s \approx 2.5$ mW/cm^2 for the transitions used) is the forward ($j = 1$) (backward, $j = 2$) pump field Rabi frequency, Δ is one-photon detuning, $\nu_r = 3.75$ kHz is rubidium atom one-photon recoil frequency. The exponential factors in Eq. (1) include the contributions from atomic c.m. motion.

In the Raman-Nath regime, the pulsed optical grating is considered to be instantaneous and atomic motion is neglected. Thus, all exponential factors are replaced by unity. Consequently, the momentum distribution of the condensate components is characterized by the Bessel functions of order n [1–11]. When the optical grating is pulsed for an appreciable time, however, deviation from the Raman-Nath approximation becomes important and the exponential factors in Eq. (1) must be included. This results in non-negligible corrections due to atomic c.m. motion. We show below that this correction is at the root of the observed condensate momentum oscillation and full matter-wave self-imaging with a period that is different from the fractional and integral Talbot time reported previously [15].

In general, Eq. (1) cannot be solved analytically. The physical origin of the observed condensate self-imaging, however, can be understood by rearranging Eq. (1) as

$$\Psi_n(p;t) = iZ[\Psi_{n-1} + \Psi_{n+1}] + iZ[\Psi_{n-1}(e^{i\delta_- t} - 1) + \Psi_{n+1}(e^{i\delta_+ t} - 1)]. \qquad (2)$$

It can be shown that in the Raman-Nath limit where the second square bracket, which represents the contribution from the atomic c.m. motion, is neglected, Eq. (2) yields

the result for a pulse time τ_P,

$$\Psi_n(p;\tau_P) = e^{ix} i^n J_n(x) \Psi_n^{(0)}, \tag{3}$$

where $x = Z\tau_P/2$, $\Psi_n^{(0)} = \sqrt{\delta(p + 2n\hbar k_L)}$ and the Dirac δ function enforces the even-photon processes. Thus, the population of the nth-order diffracted component (corresponds to $2n\hbar k_L$ momentum) is $P_n = \int_{-\infty}^{+\infty} dp |\Psi_n(p;\tau_P)|^2 = [J_n(x)]^2$ as it should be.

When the atomic c.m. motion is included the second square bracket in Eq. (2) leads to a solution of the atomic ground state population amplitude of the form

$$\Psi_n(p;\tau_P) = e^{ix} i^n [\Psi_n^{(0)} J_n(x) + G_n(\epsilon, x, \Psi_{n+m}^{(0)})], \tag{4}$$

where $\epsilon = \nu_r/Z$. We note that $G_n(\epsilon, x, \Psi_{n+m}^{(0)})$, where $|m| \leq (n+1)$, is a complex function containing the sum (over integer m) of integrals of high-order Bessel functions. Although the exact analytic expression of $G_n(\epsilon, x, \Psi_{n+m}^{(0)})$ cannot be obtained, its physical implication is clear and sufficient for one to understand the experimental observations.

In the Raman-Nath limit, the condensate momentum distribution oscillations in the time domain are solely determined by the minima of the Bessel functions given in Eq. (3). Based on the properties of Bessel functions one concludes that full matter-wave self-imaging cannot occur in the Raman-Nath regime [see Fig. 3(c) and discussion below).

In the non-Raman-Nath regime, where Eq. (2) applies, the non-negligible atomic c.m. motion leads to an interference, and the collapse and revival of the condensate momentum distribution are now determined by the minima of the quantity in the square bracket in Eq. (4). The physical meaning of the function $G_n(\epsilon, x, \Psi_{n+m}^{(0)})$ is that it modifies and shifts minima of the diffraction amplitudes as a function of pulse duration, and therefore permits the possibility of simultaneously achieving minima of all $n \geq 1$ order diffraction amplitudes. We emphasize that simultaneously achieving minima of all *high-order* amplitudes is a prerequisite for a full matter-wave self-imaging where the population distribution collapses completely to a condensate of zero momentum ($0\hbar k_L$).

The observed full matter-wave self-imaging is different from the temporal matter-wave Talbot effect reported before [15]. In the temporal matter-wave Talbot effect, two successive optical gratings are pulsed on for such a short time ($\tau_P \approx 100$ ns) that the effect of the atomic c.m. motion is totally negligible during the grating irradiation time. The condensate self-imaging is achieved by the alignment and antialignment of the atomic optical Bloch vector which precesses in the ''absence'' of any external field.

We have numerically integrated Eq. (1) to obtain the diffraction probabilities for the first few significant diffraction orders. Figure 3(a) shows that at $\tau_P \approx 23$ μs the zeroth-order diffraction probability is near 100%, whereas all high orders are very small. This agrees well with the observed time of $\tau_P = 25$ μs when all $n \geq 1$ orders are very small.

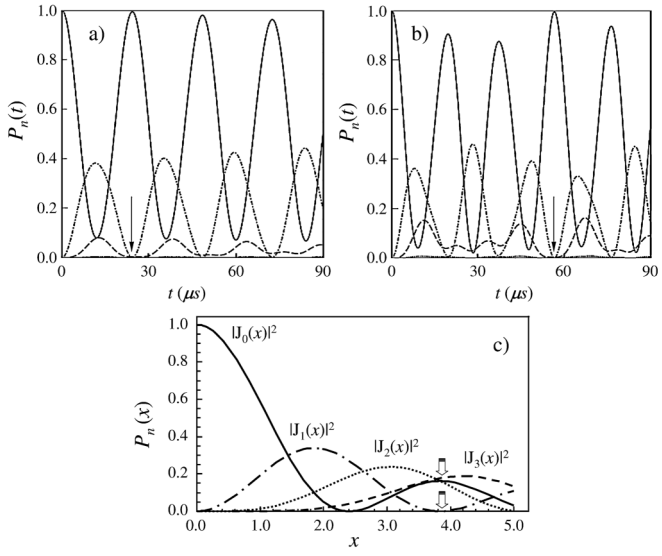

FIG. 3. (a) Probabilities of nth-order diffraction as a function of pulse duration. The numerics were done with $-3 \leq n \leq +3$ and $C_{-4} = C_4 = 0$ (calculation with $n = \pm 5$ have yielded the same results). Parameters are chosen so that $\Omega_1\Omega_2/(2\nu_r\Delta) = 25$, which is very close to the experimental value of 22. The matter-wave self-imaging occurs at $t = \tau_P \approx 23$ μs (see arrow). Solid curve, $n = 0$; dash-dotted curve, $n = 1$; dashed curve, $n = 2$; dotted curve (not visible), $n = 3$. (b) Probabilities of nth-order diffraction as a function of pulse duration for $\Omega_1\Omega_2/(2\nu_r\Delta) = 34$. The first full matter-wave self-imaging point occurs at $t = \tau_P \approx 56$ μs and partial collapses of momentum distribution can be seen [curve styles are the same as in (a)]. We note that the full matter-wave self-imaging effect due to atomic c.m. motion is characterized *only* by an interference that simultaneously minimizes all $n \geq 1$ diffraction orders and maximizes the zeroth diffraction component. (c) Raman-Nath limit diffraction probability $P_n = |J_n(x)|^2$ with $n = 0, \ldots, 3$ as functions of dimensionless argument x. Note that $|J_0(x)|^2$ reaches a maximum *again* when $|J_1(x)|^2$ becomes zero (see the arrows), indicating the simultaneous disappearance of the first-order diffraction and repopulation of the zeroth-order diffraction even when the atomic c.m. motion is neglected. At the same x, however, $n > 1$ diffraction components are significant.

Figure 3(b) shows the numerically calculated diffraction probabilities for $\Omega_1\Omega_2/(2\nu_r\Delta) = 34$. It is interesting to notice that the first full matter-wave self-imaging time moves to $\tau_P \approx 56$ μs. In addition, partial collapse of selected diffraction orders, a phenomenon that is well known in near-field imaging, are seen before the first full self-imaging is achieved. This indicates that the two-photon Rabi frequency can shift the time location of the first full matter-wave self-imaging, raising the possibility of coherently controlled and time-tunable full matter-wave self-imaging [22].

It is instructive to explain the key enabler of the matter-wave self-imaging effect. First, we point out that the full matter-wave self-imaging stems out of the non-negligible atomic c.m. motion in the non-Raman-Nath regime.

Second, observation of the simultaneous disappearance of the first-order diffraction and the repopulation of the zeroth-order diffraction does not lead to the conclusion of matter-wave self-imaging. In fact, one can show [Fig. 3(c)] that even in the Raman-Nath regime the disappearance of the first-order diffraction indeed coincides with the repopulation of the zeroth-order diffraction. This is due to the properties of the Bessel functions, not the atomic c.m. motion induced interference. However, the higher ($n > 1$) diffraction orders in this regime are not small, indicating the lack of matter-wave self-imaging. We emphasize that the key indicator of the full matter-wave self-imaging is the simultaneous minimization of all *higher* orders (not just $n = 1$ order) and maximization of the zeroth-order. This indicator is clearly shown in our work [23]. For this reason we believe that we have demonstrated for the first time a full matter-wave self-imaging effect.

Finally, we comment on the apparent asymmetry exhibited in the images shown in Fig. 2. In this work, we study momentum oscillation of a condensate as a function of atomic center-of-mass motion in a pulsed optical grating formed by counterpropagating beams with a significant intensity difference propagating along the long axis of the condensate. These two new features along with the beam propagation geometry have profound consequences. At certain interaction time we have observed that high-order components are stronger than the lower order diffraction components. This is to be expected as in near-field optical imagining multiple near-field imaging planes can be observed in which high-order components are stronger than low-order components [15]. Other causes of asymmetry stem out of the ac Stark shifts associated with uneven beam intensities and matter-wave superradiant effects [24]. Both of these effects can make the asymmetry described above more pronounced. For instance, the far-detuned strong beam leads to a matter-wave superradiant effect that favors forward scattering (i.e., $+n$ orders in the direction of the strong beam) [24]. This weak matter-wave amplification feature has never been studied in near-field atom optics.

It is important, however, to realize that these effects, which are important for accurate atom number distribution predictions, do not have significant bearing on the matter-wave self-imaging point in time. This is because the self-imaging is mainly the work of an instantaneous Doppler-shift induced interference. Thus, for the purpose of demonstrating the matter-wave self-imaging effect, the theoretical model given in Eq. (1) is sufficient. It provides a simple but reasonably accurate picture of the underlying physics and explains satisfactorily the observed matter-wave self-imaging time. It is, however, incapable of providing an accurate count of numbers of atoms in individual diffraction peaks since we have neglected ac Stark shifts, matter-wave superradiant effects, and the weak beam absorption. A detailed prediction of numbers of atoms in each diffraction peak requires a full numerical simulation beyond the scope of this work that must include these effects.

In conclusion, we have studied matter-wave momentum oscillations in a standing light wave field. We have demonstrated a new matter-wave self-imaging effect by experimentally investigating bidirectional, high-order condensate momentum distribution collapse and revival. The observed matter-wave self-imaging results from an atomic c.m. motion induced interference in a finite temporal optical standing wave. It is characterized by the simultaneous suppression of all higher ($n \geq 1$) diffraction orders and momentum collapse into the zeroth-order condensate component.

We thank Dr. Thomas Lucatorto and Dr. Jay Vaishnav for valuable suggestions and comments. We thank Dr. Lü Baolong of WIPM for assistance. K. L and M. S. Z. acknowledge financial support by the National Natural Science Foundation of China.

[1] S. Altshuler, L. M. Frantz, and R. Braunstein, Phys. Rev. Lett. **17**, 231 (1966).
[2] R. J. Cook and A. F. Bernhardt, Phys. Rev. A **18**, 2533 (1978).
[3] A. F. Bernhardt and B. W. Shore, Phys. Rev. A **23**, 1290 (1981).
[4] P. E. Moskowitz *et al.*, Phys. Rev. Lett. **51**, 370 (1983).
[5] P. L. Gould, G. A. Ruff, and D. E. Pritchard, Phys. Rev. Lett. **56**, 827 (1986).
[6] P. J. Martin *et al.*, Phys. Rev. A **36**, 2495 (1987).
[7] P. J. Martin *et al.*, Phys. Rev. Lett. **60**, 2194 (1988).
[8] P. L. Gould *et al.*, Phys. Rev. A **43**, 585 (1991).
[9] M. Lindberg, Appl. Phys. B **54**, 467 (1992).
[10] W. Zhang and D. F. Walls, Phys. Rev. A **49**, 3799 (1994).
[11] *Atom Interferometry*, edited by P. R. Berman (Academic, San Diego, 1997).
[12] M. Kozuma *et al.*, Phys. Rev. Lett. **82**, 871 (1999).
[13] J. Stenger *et al.*, Phys. Rev. Lett. **82**, 4569 (1999).
[14] Yu. Ovchinnikov *et al.*, Phys. Rev. Lett. **83**, 284 (1999).
[15] L. Deng *et al.*, Phys. Rev. Lett. **83**, 5407 (1999).
[16] E. W. Hagley *et al.*, Phys. Rev. Lett. **83**, 3112 (1999).
[17] E. W. Hagley *et al.*, Science **283**, 1706 (1999).
[18] L. Deng *et al.*, Nature (London) **398**, 218 (1999).
[19] We have a condensate with Thomas-Fermi radii of $r_0 = 14\ \mu$m and $L = 75\ \mu$m in the radial and axial directions.
[20] We used the D_2 line for this experiment. The D_1 line scheme corresponds more closely to Eq. (1).
[21] Equation (1) neglects any attenuation of the weak counterpropagating beam. It also neglects any presence of matter-wave superradiant effects and ac Stark shifts.
[22] Studies of ac Stark shifts, matter-wave superradiant effect and weak amplification, and coherently controlled full matter-wave self-imaging will be reported later.
[23] We note that due to the conditions of the setup, the experiment reported in Ref. [14] did not exhibit any observable $n > 1$ diffraction orders and therefore is incapable of demonstrating matter-wave self-imaging effect.
[24] S. Inouye *et al.*, Science **285**, 571 (1999); R. Gonifacio *et al.*, Opt. Commun. **233**, 155 (2004); Özgür E. Müstecaplioğlu and L. You, Phys. Rev. A **62**, 063615 (2000).